

---

# Generative Modelling of Rough Surfaces: An Application to 3D-Printed Stainless Steel

---

Anonymous Author(s)

Affiliation

Address

email

## Abstract

1 The emergence of 3D printing technologies for stainless steel enables steel struc-  
2 tures with almost arbitrarily complex geometries to be manufactured. A com-  
3 mon design preference for steel structures is that they are *thin-walled*, to reduce  
4 weight and limit the requirement for raw material. The mechanical properties  
5 of thin-walled structures are principally determined by their geometry; however,  
6 3D-printed steel components exhibit geometric variation beyond that which was  
7 intended, due to the welding process involved, at a scale that is non-negligible  
8 with respect to the thickness of the wall. The cumulative impact of geometric  
9 variation is to alter the macro-scale mechanical properties of a printed component,  
10 such as deformation under load. An important challenge is therefore to predict the  
11 (random) macro-scale mechanical properties of a component, before it is manu-  
12 factured. To address this, we trained a generative probabilistic model for rough  
13 surfaces defined on smooth manifolds to an experimentally-obtained dataset con-  
14 sisting of samples of 3D-printed steel. Combined with finite element simulation of  
15 components under load, we were able to produce detailed probabilistic predictions  
16 of the mechanical properties of a 3D-printed steel component. The main technical  
17 challenge was to transfer information from the training dataset to the hypothetical  
18 component, whose notional geometry may be described by a different manifold.  
19 Our proposed solution was to employ spatial random field models which can be  
20 characterised *locally* using a differential operator, and to leverage the correspon-  
21 dence between the Laplacian on the training and the test manifolds to facilitate the  
22 transfer of information.

## 1 Introduction

24 Much study has been devoted to the field of surface metrology; the science of rough surfaces. Ef-  
25 fective characterisation of uneven and imperfect surfaces is paramount to the physical disciplines of  
26 tribology and structural analysis of thin walled components, as the nature and distribution of imper-  
27 fections have major effects of the behaviour of components under both contact and stress conditions.  
28 Traditionally, surfaces were characterised using a number of quantitative measures defined by the  
29 distribution of peaks, troughs and their distance [12]; with more sophisticated approaches utilising  
30 such information to create ARMA or spectral descriptions of analysed surface profiles [13, 4, 7].  
31 Comparatively less study has been devoted to creating generative models and even less attention has  
32 been devoted to fitting such models to data [9, 2]. This conference abstract examines utilising laser  
33 scan data of 3D printed stainless steel samples to create a generative model of the surface, for any  
34 component that could in principle be manufactured. This is of great interest as 3D printed stainless  
35 steel has the potential to enable the construction of complex and efficient structures, which would  
36 otherwise be difficult or impossible to fabricate [3]. To this end we constructed a flexible model, able

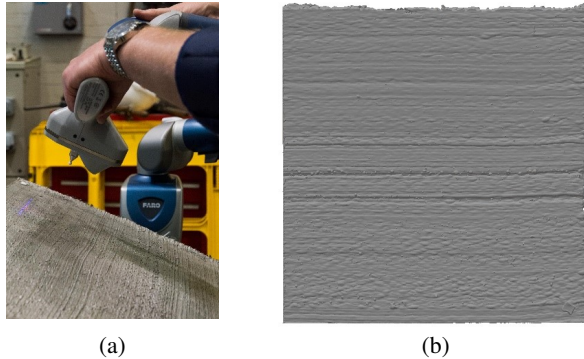


Figure 1: Laser scan of 3D-printed steel sheet. (a) Photograph of the handheld scanning equipment. (b) A scanned portion of the sheet, which we call a *panel*. The notional thickness of the panel is 3.5mm.

37 to describe the geometry of any hypothetical component, notionally defined by a two-dimensional  
 38 manifold  $\mathcal{M}$  embedded in  $\mathbb{R}^3$ . The approach is described next.

## 39 2 Methodology

### 40 2.1 Characteristics of the Training Dataset

41 Data were obtained from six separate laser scans of an experimentally produced, notionally flat,  
 42 3D-printed steel sheet, courtesy of [source blinded for review]. See Figure 1b. The resultant three-  
 43 dimensional data panels were then flattened to remove a small global trend<sup>1</sup>, and digitally processed  
 44 to remove small beads of splatter, which occurs on occasion but does not affect mechanical proper-  
 45 ties of interest. The result is a pair of matrices representing the height of the upper and lower faces  
 46 of the material from its notional defining manifold. See Figure 2a. The high resolution (< 1mm) of  
 47 the laser scan suggests we can treat these data as noiseless evaluations from a pair of scalar-valued  
 48 functions,  $u_1(x)$  and  $u_2(x)$ , defined on a manifold  $\mathcal{M}$  which is embedded in  $\mathbb{R}^3$ .

### 49 2.2 Generative Modelling of Rough Surfaces

50 The training data were used to infer the parameters of a generative model for geometric variation in  
 51 3D-printed steel. Our main requirement for a generative model is that it can handle notional geome-  
 52 tries  $\mathcal{M}$  that are possibly quite complicated, due to the considerable freedom in terms of components  
 53 that could be manufactured. This precludes the use of established covariance function representa-  
 54 tions of a spatially varying random field [10], as covariance functions are intimately related<sup>2</sup> to the  
 55 domain on which they are defined [5]. Instead, we note that a wide range of random fields can be  
 56 described by solution of a stochastic partial differential equation (SPDE) with a differential operator  
 57 based on the Laplacian  $\Delta_{\mathcal{M}}$  of the manifold  $\mathcal{M}$  [see e.g. 8]. These differential operators are defined  
 58 locally only and thus, if we are willing to associate the Laplacian  $\Delta_{\mathcal{M}}$  on one manifold with the  
 59 corresponding Laplacian  $\Delta_{\mathcal{M}'}$  on another manifold, then conclusions drawn from data obtained on  
 60  $\mathcal{M}$  can be used to inform a generative model for random fields on  $\mathcal{M}'$ .

61 To this end, we construct a SPDE model for the random fields  $u_1, u_2 : \mathcal{M} \rightarrow \mathbb{R}$ , whose parameters  
 62 we can fit to our training dataset. We note that  $u_1$  and  $u_2$  are not independent, since  $u_1 + u_2$   
 63 is the thickness of the steel wall and is notionally fixed (to 3.5mm) and we therefore follow [6]  
 64 in considering coupled systems of SPDEs to model random vector fields whose components are  
 65 correlated. Let  $\Omega$  be an underlying probability space, on which all random variables are defined, and

<sup>1</sup>This trend was due to residual stresses that were re-distributed when extracting each panel from a single larger sheet

<sup>2</sup>This is clearly illustrated by the fact that a function of the form  $k(x, y) = \phi(d_{\mathcal{M}}(x, y))$ , where  $d_{\mathcal{M}}$  is the geodesic distance on  $\mathcal{M}$ , which is positive definite for some  $\mathcal{M}$  can fail to be positive definite for other  $\mathcal{M}$ ; see [5].

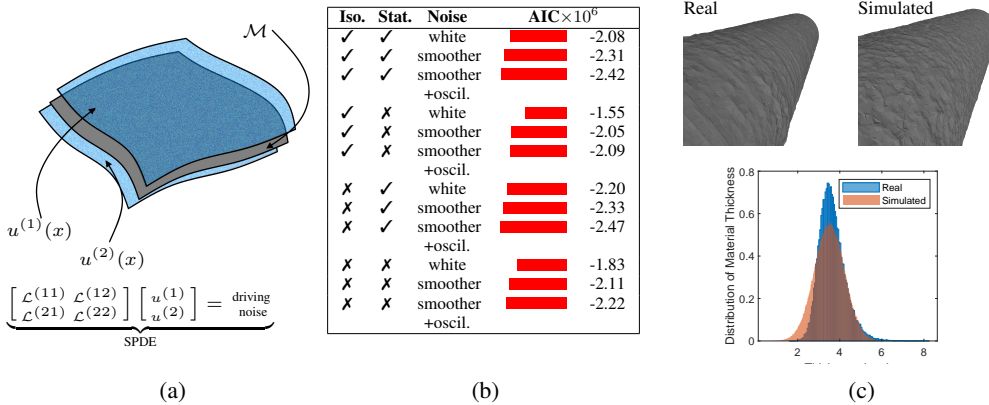


Figure 2: Generative models for 3D-printed steel: (a) A model for geometric variation was constructed using a bivariate stochastic partial differential equation (SPDE), defined on a manifold  $\mathcal{M}$  representing the notional geometry of the component. Data were conceptualised as a two-dimensional vector field  $u$  on  $\mathcal{M}$ . The value  $u^{(1)}(x)$  represents the height of the upper surface of the material above  $x \in \mathcal{M}$ , while the value  $u^{(2)}(x)$  represents the height of the lower surface below  $x \in \mathcal{M}$ . (b) Statistical model selection, based on the Akaike information criterion (AIC). [“Iso.” = isotropic, “Stat.” = stationary, “oscil.” = oscillatory.] (c) Real and simulated circular hollow sections (CHS) and the distribution of the wall thickness for a CHS.

66 let  $\omega \mapsto Z^{(r)}(x, \omega)$ ,  $r \in 1, 2$  be independent centred real-valued random fields whose distribution is  
67 to be specified, such that almost surely  $Z^{(j)} \in L^2(\mathcal{M})$ . Henceforth we leave the argument  $\omega \in \Omega$   
68 implicit. Let  $\mathcal{L}^{(rs)}$ ,  $r, s \in 1, 2$ , be differential operators on  $\mathcal{M}$ , to be specified and consider the  
69 following coupled system of SPDEs:

$$\begin{bmatrix} \mathcal{L}^{(11)} & \mathcal{L}^{(12)} \\ \mathcal{L}^{(21)} & \mathcal{L}^{(22)} \end{bmatrix} \begin{bmatrix} u^{(1)}(x) \\ u^{(2)}(x) \end{bmatrix} = \begin{bmatrix} Z^{(1)}(x) \\ Z^{(2)}(x) \end{bmatrix}, \quad x \in \mathcal{M}, \quad (1)$$

70 Neumann boundary conditions are applied on  $\partial\mathcal{M}$  and we compactly represent this system in matrix  
71 notation as  $\mathcal{L}\mathbf{u} = \mathbf{Z}$ .

72 The generative model in (1) requires that the differential operator  $\mathcal{L}$  and the driving noise process  $\mathbf{Z}$   
73 are specified. This is discussed next.

### 74 2.3 Parametrisation of the Generative Model

75 A selection of candidate models for the components of the differential operator  $\mathcal{L}$  were considered,  
76 which differed in their complexity. These included the possibility for anisotropy and non-  
77 stationarity, and are briefly summarised in Table 1.

Model for $\mathcal{L}^{(rs)}$	Mathematical Form
Isotropic Stationary	$\mathcal{L}^{(rs)}u(x) := (\eta^{(rs)} - \Delta)(\tau^{(rs)}u(x))$
Anisotropic Stationary	$\mathcal{L}^{(rs)}u(x) := (\eta^{(rs)} - \nabla \cdot \mathbf{H}^{(rs)}\nabla)(\tau^{(rs)}u(x))$
Isotropic Non-stationary	$\mathcal{L}^{(rs)}u(x) := (\eta^{(rs)}(x_3) - \Delta)(\tau^{(rs)}(x_3)u(x))$
Anisotropic Non-stationary	$\mathcal{L}^{(rs)}u(x) := (\eta^{(rs)}(x_3) - \nabla \cdot \mathbf{H}^{(rs)}\nabla)(\tau^{(rs)}(x_3)u(x))$

Table 1: Candidate models for the differential operator  $\mathcal{L}$ .

78 In the anisotropic models, the matrices  $\mathbf{H}^{(rs)}$  act as a length-scale parameter to allow separate  
79 control of the variation in the vertical coordinate  $x_3$ , which is the direction in which successive steel  
80 layers are added (and is well-defined for any component, irrespective of its notional manifold  $\mathcal{M}$ ),  
81 compared to the coordinates  $x_1$  and  $x_2$  that are in the plane of the layer structure in the material.  
82 Likewise, in the non-stationary models the coefficients  $\eta^{(rs)}$  and  $\tau^{(rs)}$  are allowed to depend on  $x_3$   
83 but not on  $x_1$  not  $x_2$ . The spatially varying coefficients  $\eta^{(rs)}$  and  $\tau^{(rs)}$  were parametrised using

- 84 a small number of Fourier basis functions, so that our models for  $\mathcal{L}$  vary in their number of free  
 85 parameters between 4 and 98.
- 86 For the driving noise  $\mathbf{Z}$  we considered three possibilities; (i) white noise, (ii) smooth noise, and (iii)  
 87 smooth noise with an oscillatory component. Our models for  $\mathbf{Z}$  vary in their number of free param-  
 88 eters between 0 and 4. A detailed description goes beyond the scope of this conference abstract, but  
 89 we note that each of these three noise models for SPDEs was previously described in [8].
- 90 The combination of 4 models for  $\mathcal{L}$  and 3 models for  $\mathbf{Z}$  leads to 12 candidate models in total. Next  
 91 we discuss the fitting of these generative models to our training dataset.

### 92 3 Results

- 93 For each candidate model, we fitted the free parameters, here denoted  $\theta$ , to the training dataset using  
 94 maximum likelihood. This required considerable computational resources, since although one can  
 95 exploit sparse Markov random field approximations to the system of SPDEs in (1) to efficiently  
 96 evaluate the Gaussian log-likelihood [8], the derivatives of this log-likelihood with respect to  $\theta$  do  
 97 not admit sparse matrix methods [11]. Our solution involved developing a bespoke approach to  
 98 optimisation that used natural gradient ascent [1] on a surrogate likelihood based on a subset of the  
 99 dataset.
- 100 Once the maximum likelihood estimators for  $\theta$  has been numerically approximated for each model  
 101 in the candidate set, we compared models using the Akaike Information Criteria (AIC; smaller  
 102 values preferred), in order to select the best model in a manner that balances goodness-of-fit with  
 103 simplicity. As measured by AIC, in Figure 2b, the anisotropic stationary model driven by a smooth  
 104 and oscillatory noise process was observed to be the best representation of the training dataset.
- 105 To test if the best candidate was able to simulate a good representation of the 3D printed stainless  
 106 steel, we looked to simulate a notional cylindrical hollow section (CHS) with the same dimensions  
 107 as a real 3D-printed component, which we held out to constitute the test dataset. Note that the CHS  
 108 corresponds to a manifold that differs from that of the training dataset. However, this CHS had the  
 109 same notional thickness as the panels in our training dataset, so that the information learned from  
 110 the dataset by the generative model ought to be transferable to the CHS. The spatial distribution  
 111 of wall thickness from a simulation from our generative model for the CHS was compared with  
 112 the distribution of wall thickness computed from the test dataset to provide a basic, but practically  
 113 relevant, opportunity to assess the performance of the fitted generative model. This test is limited  
 114 as it provides no spatial featurisation, but is easily implemented and visualised. We can see from  
 115 the comparison in Figure 2c that while the distributions are similar to one another and centred at the  
 116 3.5mm mark, the simulation failed to capture the positive skew present in the real CHS. From an  
 117 engineering perspective, these failings may not be too much of a problem as the simulated model  
 118 is more pessimistic from a thickness point of view, so shouldn't compromise the decision-making  
 119 process if the models were to be used in a safety assessment.
- 120 As small variations in geometry can have a significant impact on structural behaviour, we next  
 121 undertook a more detailed investigation and compared the results of simulated buckling tests on our  
 122 generated CHS with results obtained in a real experiment. Finite element simulation was used to  
 123 simulate axial compression of our simulated CHS, and the simulations were repeated for multiple  
 124 instantiations of the simulated CHS. The results showed behaviour similar to those observed in the  
 125 real compressive tests; see Figure 3. However, the simulated columns were more prone to sharp  
 126 bifurcations in the buckling behaviour. This could be due to a number of reasons, including mis-  
 127 specification of the physical properties of the material (e.g. the Young's modulus of 3D-printed steel  
 128 might in fact be spatially varying, whereas we assumed material properties were identical to those  
 129 of standard steel), and cannot be attributed directly to the generative geometry model.

### 130 4 Conclusion

- 131 In this conference abstract we have shown, for the first time, that it is possible to create generative  
 132 models for the geometric features of 3D-printed steel components, even when such components  
 133 have not yet been manufactured. To main challenge that we faced was to construct a model that  
 134 did not depend on the manifold on which the random fields were defined. Our main insight and

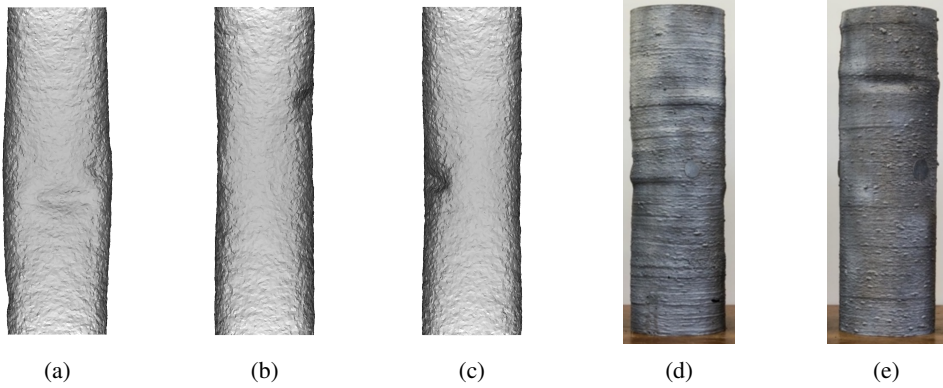


Figure 3: Predicting the outcome of a compressive test on a 3D-printed cylindrical hollow section (CHS), using the fitted generative model for the geometry of the CHS and a finite element simulation of the experiment. (a-c) Samples from the generative model for the geometry of the CHS after the simulated compressive test. (d-e) Buckled CHS, experimentally produced. Reproduced with permission from [blinded for review].

135 proposed solution was to represent our random fields as solutions to a system of coupled SPDEs  
 136 whose differential operator characterisation is only locally defined. Model selection was performed  
 137 over a set of candidates and resulted in the choice of a generative model which exhibited anisotropy  
 138 and was driven by a smooth and oscillatory noise process. This model, fitted on training data from  
 139 notionally flat panels, was used to generate geometries for notional CHS, with dimensions matching  
 140 an existing 3D-printed CHS that was held out as a test set. A preliminary validation of the model was  
 141 performed in this context, using finite element simulation to recreate a compressive test. Evidently  
 142 this modelling approach can be further developed and this presents a promising avenue for further  
 143 research into generative modelling of rough surfaces, that is likely to have engineering applications  
 144 beyond 3D-printed steel.

#### 145 Acknowledgements

146 [blinded for review]

#### 147 References

- 148 [1] Shun-Ichi Amari. Natural gradient works efficiently in learning. *Neural Computation*,  
 149 10(2):251–276, 1998.
- 150 [2] Vasilios Bakolas. Numerical generation of arbitrarily oriented non-gaussian three-dimensional  
 151 rough surfaces. *Wear*, 254(5):546 – 554, 2003.
- 152 [3] C Buchanan and L Gardner. Metal 3d printing in construction: A review of methods, research,  
 153 applications, opportunities and challenges. *Engineering Structures*, 180:332–348, 2019.
- 154 [4] R. E. DeVor and S. M. Wu. Surface Profile Characterization by Autoregressive-Moving Average  
 155 Models. *Journal of Manufacturing Science and Engineering*, 94(3):825–832, 08 1972.
- 156 [5] Tilman Gneiting. Strictly and non-strictly positive definite functions on spheres. *Bernoulli*,  
 157 19(4):1327–1349, sep 2013.
- 158 [6] Xiangping Hu, Finn Lindgren, Daniel Simpson, and Håvard Rue. Multivariate Gaussian ran-  
 159 dom fields with oscillating covariance functions using systems of stochastic partial differential  
 160 equations. *arXiv preprint arXiv:1307.1384*, 2013.
- 161 [7] Y.Z. Hu and K. Tonder. Simulation of 3-d random rough surface by 2-d digital filter and  
 162 fourier analysis. *International Journal of Machine Tools and Manufacture*, 32(1):83 – 90,  
 163 1992. Proceedings of the 5th International Conference on Metrology and Properties of Engi-  
 164 neering Surfaces.

- 165 [8] Finn Lindgren, Håvard Rue, and Johan Lindström. An explicit link between Gaussian fields  
166 and Gaussian Markov random fields: the stochastic partial differential equation approach.  
167 *Journal of the Royal Statistical Society: Series B (Statistical Methodology)*, 73(4):423–498,  
168 2011.
- 169 [9] Nadir Patir. A numerical procedure for random generation of rough surfaces. *Wear*, 47(2):263  
170 – 277, 1978.
- 171 [10] C.E. Rasmussen and C.K.I. Williams. *Gaussian Processes for Machine Learning*. MIT Press,  
172 2006.
- 173 [11] Sam Davanloo Tajbakhsh, Necdet Serhat Aybat, and Enrique Del Castillo. Sparse precision  
174 matrix selection for fitting gaussian random field models to large data sets. *arXiv preprint*  
175 *arXiv:1405.5576*, 2014.
- 176 [12] Tom R Thomas. Rough surfaces. *Rough Surfaces, 2nd Edition. Edited by THOMAS TOM R.*  
177 *Published by World Scientific Publishing Co. Pte. Ltd., ISBN# 9781860943805*, 1999.
- 178 [13] Jiunn-Jong Wu. Simulation of rough surfaces with fft. *Tribology International*, 33(1):47 – 58,  
179 2000.